International Journal of Surface Engineering and Interdisciplinary Materials Science
Volume 9 • Issue 2 • July-December 2021

Correlative Analysis Between Tensile Properties and Tool Rotational Speeds of Friction Stir Welded Similar Aluminium Alloy Joints

Velaphi Msomi, Cape Peninsula University of Technology, South Africa
https://orcid.org/0000-0002-5752-8848

Busiswa Tracey Jantjies, Cape Peninsula University of Technology, South Africa

ABSTRACT

Friction stir welding (FSW) is considered as the new joining technique which does not involve fumes like any traditional joining techniques. The attainment of good weld depends on proper combination of FSW parameters, and this combination varies with the materials that are being welded. The tool rotational speed is known as the most critical parameter towards the generation of heat required to produce the weld in friction stir welding. This parameter plays an important role in restructuring the stir zone. The variation of this parameter may yield certain results which are dependent on the type of materials being welded. This paper reports on the impact of the rotational speed variation on the tensile properties of AA6082-T6 joints. The rotational speed was varied while keeping all the other welding parameters constant. The analysis was performed comparatively on the specimens that were sampled from different locations of the joint. The joints produced through the rotational speed of 600 rpm showed good tensile properties compared to joints produced through other rotational speeds.

KEYWORDS

Friction Stir Welding, Microhardness, Microstructure, Tensile Properties, Tool Rotational Speed

INTRODUCTION

Metal joining techniques are categorized into two main groups i.e. fusion and solid-state welding. Categorizing these techniques depends on the operating principle of each welding. Friction stir welding (FSW) is one of the techniques that fall under the solid-state welding category. The invention of this technique is associated with The Welding Institute (TWI) from the United Kingdom in the early 1990s, (Unnikrishnan & Dhas, 2017). The earlier application of FSW is mostly linked with joining soft metals such as aluminum alloys, copper, etc. These materials were known to be not weldable through fusion techniques as they possess a low melting temperature (Adamowski et al., 2007). FSW operating principle does not produce smoke or fume hence it is described as green technology (Bozorgzadeh & Idris, 2015; Mishra & Ma, 2005).

Friction stir welding joins materials through the use of a non-consumable rotating tool which generally has a specific pin and shoulder. This rotating tool is plunged between the materials to be joined and settles for a short time (dwell time). After elapsing the dwell time, the tool moves parallel

DOI: 10.4018/IJSEIMS.2021070104

to the plates being joined i.e. from the beginning to the end of the plates. The rotating tool softens and mixes the plasticized material. The joint is formed by the restricted material movement caused by the tool shoulder (Ahmed et al.,2020; Silva-Magalhaes et al., 2019). Friction stir welding is considered to have reached a stationary state when the quality of the weld is the same throughout the weld (Kumar et al., 2020; Ratnam et al., 2019; Tongne et al., 2016; Yang et al., 2019). Various works have been done in evaluating the impact of different welding parameters on the quality of joints. This includes the rotational speed, welding speed, tool tilt angle, pin profiles, and many more. The evaluation of these parameters includes the similar and dissimilar materials (Raturi et al., 2019; Thilagham & Muthukumaran, 2020; Chanakyan et al., 2020; Swaminathan et al., 2020; Kumar & Ramana, 2020).

Boccarusso et al. (2019) have evaluated the impact of the welding force on the microstructural arrangement of a 3 mm thick AA6082/AZ31 Mg dissimilar joint. The H13 steel tool with 13 mm diameter concave shoulder and 3.7 mm long threaded tapered pin was used in welding the two dissimilar materials. The FSW was performed using different rotational speeds and the traverse speed. The investigation of force influence was studied in conjunction with speed variations. The presence of the hard intermetallic compounds on the weld bead was observed. These intermetallic compounds were found to be influencing the microhardness at the stir zone. The vertical force was found to have more influence on the occurrence of liquation phenomenon. Maneiah et al. (2020) used the Taguchi method in performing FSW parametric optimization using the AA6061 plate. The rotational speed, tool tilt angle, and the traverse speed were the parameters considered for this study. The H13 tool steel with 20 mm shoulder diameter and 3 mm long hexagonal pin was used in producing the welds. It was discovered that the tensile strength is influenced mostly by the factor feed than the tilt angle and the rotational speed. The optimum parameters suitable for high tensile strength of the joint were also discovered

The influence of the rotational speed on the joint formed from the as-received and the preheated AA6082 was investigated by Ciccarelli et al. (2018). The high rotational speed ranging between 1000 and 2500 rpm was used. The H13 tool steel with 12 mm shoulder diameter and 3.5 cone base diameter with 1.7 mm height was used in this study. The maximum rotational speed of 2000 rpm was found to be the best speed to produce the highest ultimate tensile strength (UTS) of preheated AA6082 while 1500 rpm was found to be the optimum speed to produce high UTS for as-received AA6082 joint. The distinct optimum speed is linked to the difference in the mechanical properties of the base metals. Swaminathan & Sathiyamurthy (2020) have performed the impact of various welding parameters on different properties of the dissimilar joint. The parameters that were varied in this study involved the vertical force, welding, and tool rotational force. Four different pin profiles were utilized in this investigation and those profiles being cylindrical, tapered-threaded, triangular, and square-shaped profiles. It was discovered that the tool rotational speed plays a major role in the enhancement of the tensile properties of the joint. The triangular pin profile produced the joint with the highest tensile strength at a rotational speed of 1000 rpm.

The impact of tool rotational speed towards the dissimilar joint properties was investigated by Zhang et al. (2020). The rotational speed range for this study was between 600 rpm and 1650 rpm, with an interval of 350 rpm. The 15 mm shoulder diameter tool with a 5 mm long tapered pin was used in this investigation. The low tool rotational speed was found to have fine grains compared to the base metal. The increase in rotational speed was found to have an adverse impact on the stir zone grain size. The influence of rotational speed on dissimilar joints depends also on the positioning materials being used in joint formation. This then suggests it is imperative to consider the material positioning when the parametric study is performed on dissimilar joints (Raturi et al., 2019; Da & Toppo, 2018; Guo et al.,2019; Sunilkumar,2020; Acharya,2020; Nagu & Humar,2020; Palani et al., 2018). The tool rotation speed plays a major role in the refinement of the grain size at the stir zone and this contributes towards the enhancement of the tensile properties of the joint. The grain size geometry is influenced by the heat input generated during the welding process and the grains with the same size tends to face in the same direction (Moshwan et al., 2015; Ahmadi et al.,2012; Ramnath et al.,2018; Sharma & Dwivedi, 2017).

It was observed that the majority of works being reported around the variation of tool rotational speed generally incorporates the other variables during the investigation. Some involve either the pretreatment of the materials or the use of dissimilar materials. This makes it difficult to understand exactly the impact of this parameter on the as-received material. It is further important to note that the impact of varying any FSW parameter also depends on the tool profile and the materials being welded. To the best knowledge of the authors, there is no available literature that analyzed the influence of the low rotational speed on the tensile strength of AA6082-T6 similar joint. This paper critically analyzed the impact of low tool rotational speed towards the tensile properties of AA6082-T6 similar joint. All other parameters were kept constant while the tool rational speed was varied. Moreover, the comparative analysis is performed on the specimens extracted from various locations of the joint as this was found to be crucial (Msomi and Mbana, 2020).

EXPERIMENTAL PROCEDURE

The as-received 6 mm thick AA6082-T6 plate was cut into 500 mm x 70 mm (length x breadth) dimensions to fit in the backing plate. The dimensioned plates were fixed on the backing plate of the semi-automated milling machine for welding (see Figure 1). The chemical composition of the AA6082-T6 is shown in Table 1. The H13 steel tool with a threaded-cylindrical pin profile was utilized in this study (see Figure 2). The dimensions of the tool are shown in Table 2. The welding parameters used in this study are shown in Table 3. It should be noted that the rotational speed was the only varying parameter in performing the welding. At least three plates were produced in each set of parameters and the macrostructural morphology of the joint was used in selecting the plates for analysis. The length of the weld was kept at approximately 480 mm which is less than the length of the plates. The traverse speed and the tilt angle were chosen based on the trial runs that were performed before resuming the actual study. The properties of the joint were analyzed through various tests that were performed using relevant standards. This includes tensile tests, microstructural analysis, fracture morphology, and microhardness tests. Waterjet technology was used in preparing specimens for the mentioned tests and all the specimens were cut perpendicular to the welding direction. The tensile tests were conducted using the Hounsfield tensile testing machine with QMAT software. The tensile specimens were prepared and tested based on the ASTM-E8M-04 standard. The fractured surface post tensile tests were analyzed using the scanning electron microscopy (SEM). The InnovaTest Falcon 500 machine was used to perform a microhardness test based on the ASTM-E384-11 standard. The 10s dwell time and 300 g load were the parameters used in conducting microhardness across the joint. The Motic AE2000 optical microscopy was used in conducting the microstructural analysis of the different zones of the samples through the guidance of ASTM-E-112 standard. Before performing microstructural analysis, the specimens were etched using Weck’s etchant. The linear intercept method through ImageJ software was employed in measuring grains. It should be noted that three specimens were prepared from each plate i.e. start (S), middle (M), and end (E) of the plate and these specimens were studied comparatively.

RESULTS AND DISCUSSION

Macroscopic View of the Joints

The influence of the increase in rotational speed on the macrostructure of the joints is shown in Figure 3-5. Figure 3 shows the surface of the joints for specimens sampled at the beginning of the weld for all the rotational speeds i.e. 600 rpm (S1), 700 rpm (S2), 800 rpm (S3), 900 rpm (S4), 1000 rpm (S5), 1200 rpm (S6). The characteristic zones associated with FSW are visible in all the surfaces i.e. stir

Figure 1. The dimensioned plates were fixed on the backing plate of the semi-automated milling machine for welding

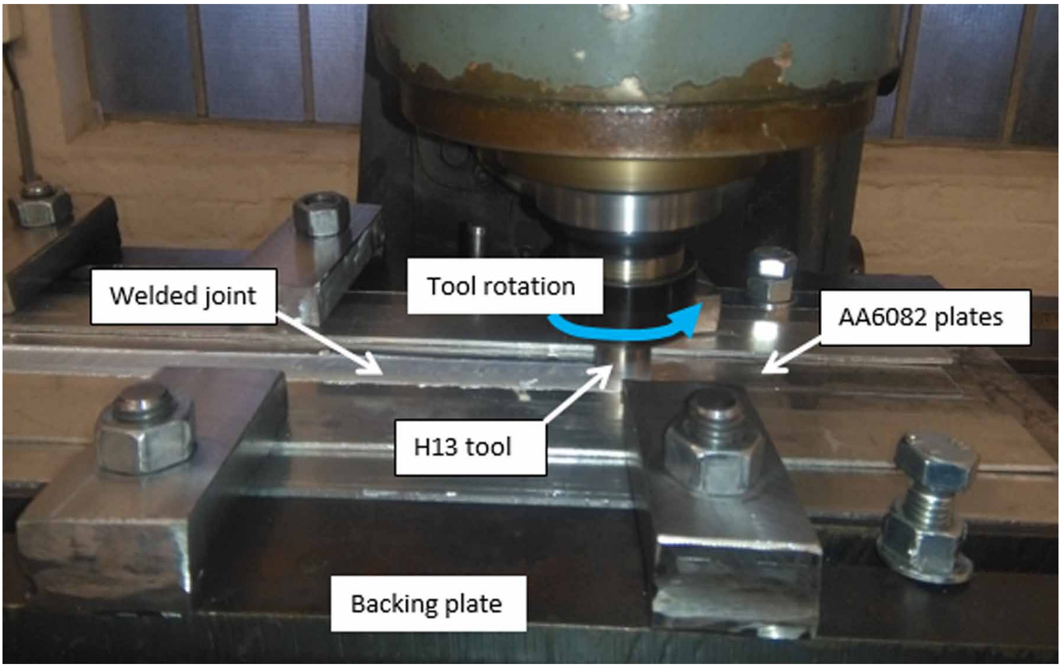

zone (SZ), thermos-mechanically affected zone (TMAZ), and heat affected zone (HAZ). The trace of tool pin disruptive mechanical action called onion rings can be seen in Figure 3 (S1)-(S4) but fades away in Figure 3 (S5) and (S6). The fading away of the onion rings is assumed to be caused by excessive heat that is generated at a high rotational speed. The presence of onion rings also suggests the material flow and proper intermixing resulting from the stir action (da Silva et al., 2011). Figure 3 (S1) and (S3) show the presence defects or wormholes and these defects are caused by improper

Figure 2. The H13 steel tool with a threaded-cylindrical pin profile was utilized in this study

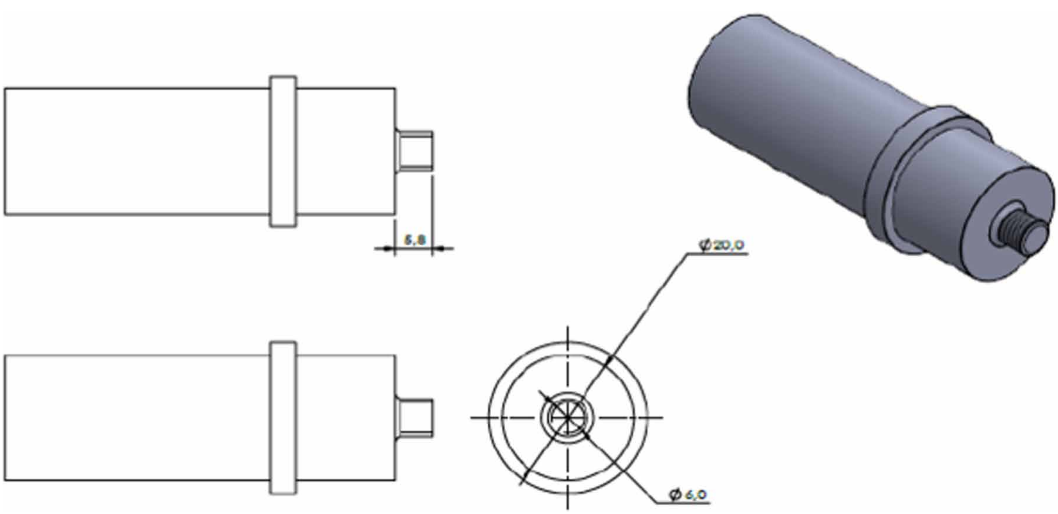

Table 1. Chemical Composition of AA6082-T6 (Sameer & Birru 2019)

	Contributing elements (wt %)							
Material	Mg	Zn	Cr	Si	Mn	Fe	Cu+Ag	Al
AA6082-T6	1.1	0.20	0.25	0.90	0.70	0.50	0.10	Bal

Table 2. Tool dimensions (Msomi et al., 2020)

Profile	Shoulder diameter (mm)	Pin diameter (mm)	Pin length (mm)
Threaded-cylindrical	20	6	5.8

mixing that occurred at the beginning of the joint (Taheri et al., 2019; Safeen & Spena, 2019). The flash structures are visible on the surface of the joint and the produced at higher rotational speed (S5) and (S). The existence of these structures is caused by too much-plasticized material escaping from the bottom of the pin shoulder. This phenomenon is caused by material bending which results from excessive heat input. Figure 4 shows the surfaces of the joints for specimens sampled in the middle of the weld for all the rotational speeds. The characteristic regions observed in Figure 3 are also identified in Figure 4. However, the defects observed in some surfaces of Figure 3 are not visible in Figure 4 and this suggests stability in heat input which encouraged the proper mixing at the stir zone (Msomi&Mbana, 2020; Zhang et al., 2019). The macrostructural appearance of the specimens sampled at the end of the plate for all the speeds is shown in Figure 5. The zones identified in Figure 4 are also present in Figure 5. Additionally, some surfaces in Figure 5 show oxide alignment which is normally associated with an excessive heat input experienced during welding (Soni et al., 2017).

Microstructural Analysis

The grain size analysis was performed at the three zones (SZ, TMAZ, and HAZ) of the weld and three locations of each plate (start, middle, and the end of the weld). There were 30 readings recorded

Table 3. Experimental parameters for FSW

Rotational speed (rpm)	Welding speed (mm/min)	Tool tilt angle (°)	Dwell time(s)
600	80	2	10
700	80	2	10
800	80	2	10
900	80	2	10
1000	80	2	10
1200	80	2	10

Figure 3. Surface of the joints for specimens sampled at the beginning of the weld for all the rotational speeds i.e. 600 rpm (S1), 700 rpm (S2), 800 rpm (S3), 900 rpm (S4), 1000 rpm (S5), 1200 rpm (S6)

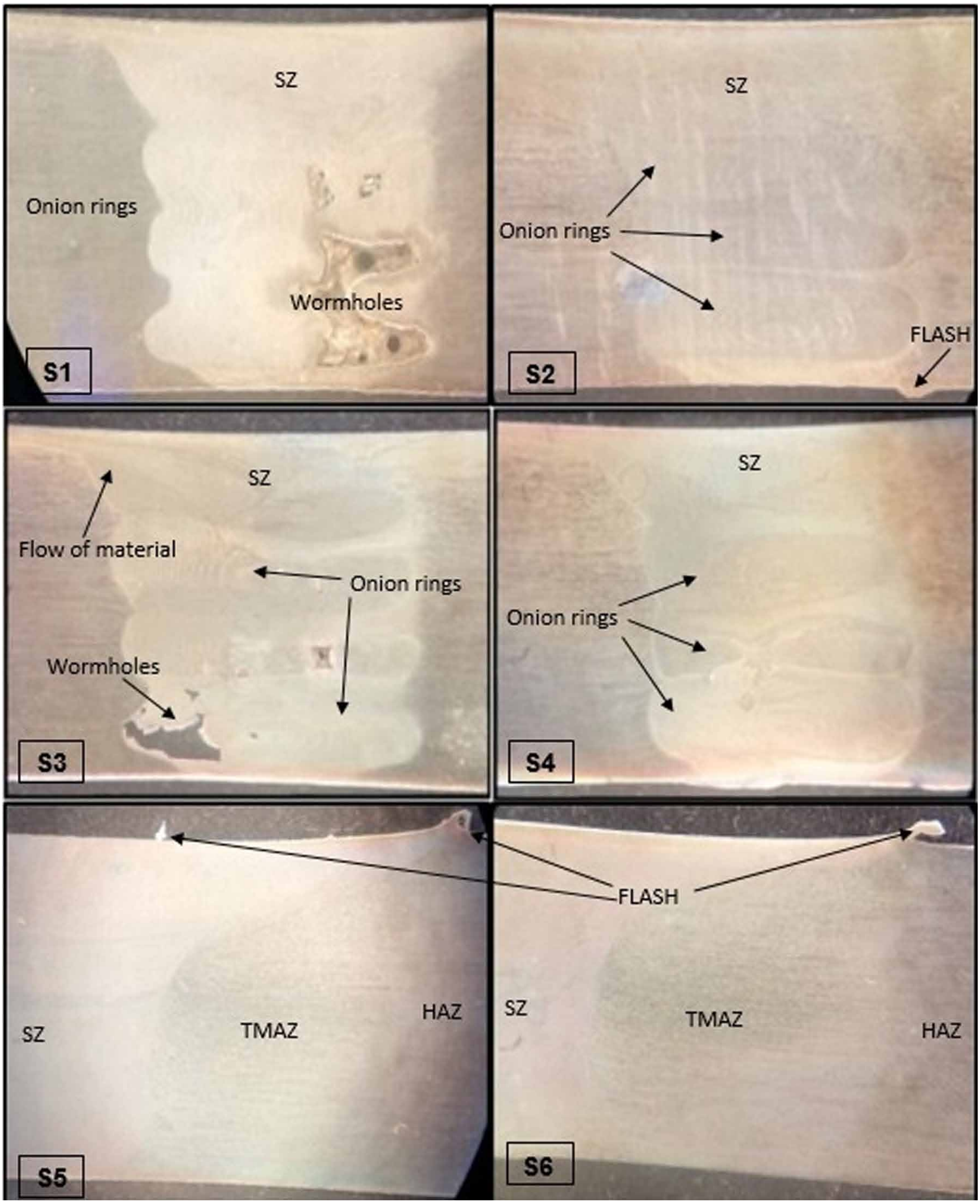

per zone of each specimen hence the inclusion of error bars in figures. The average grain size for the specimens sampled from the start on the weld of all the speeds is shown in Figure 6(a) while Figure 6(b) and (c) present the average grain size of specimens sampled from the middle and the end of the weld. The average grain size at the stir zone remains remarkably smaller compared to the average grain size at the TMAZ and HAZ regions for all the specimens sampled from different locations of the weld.

Figure 4. Surfaces of the joints for specimens sampled in the middle of the weld for all the rotational speeds

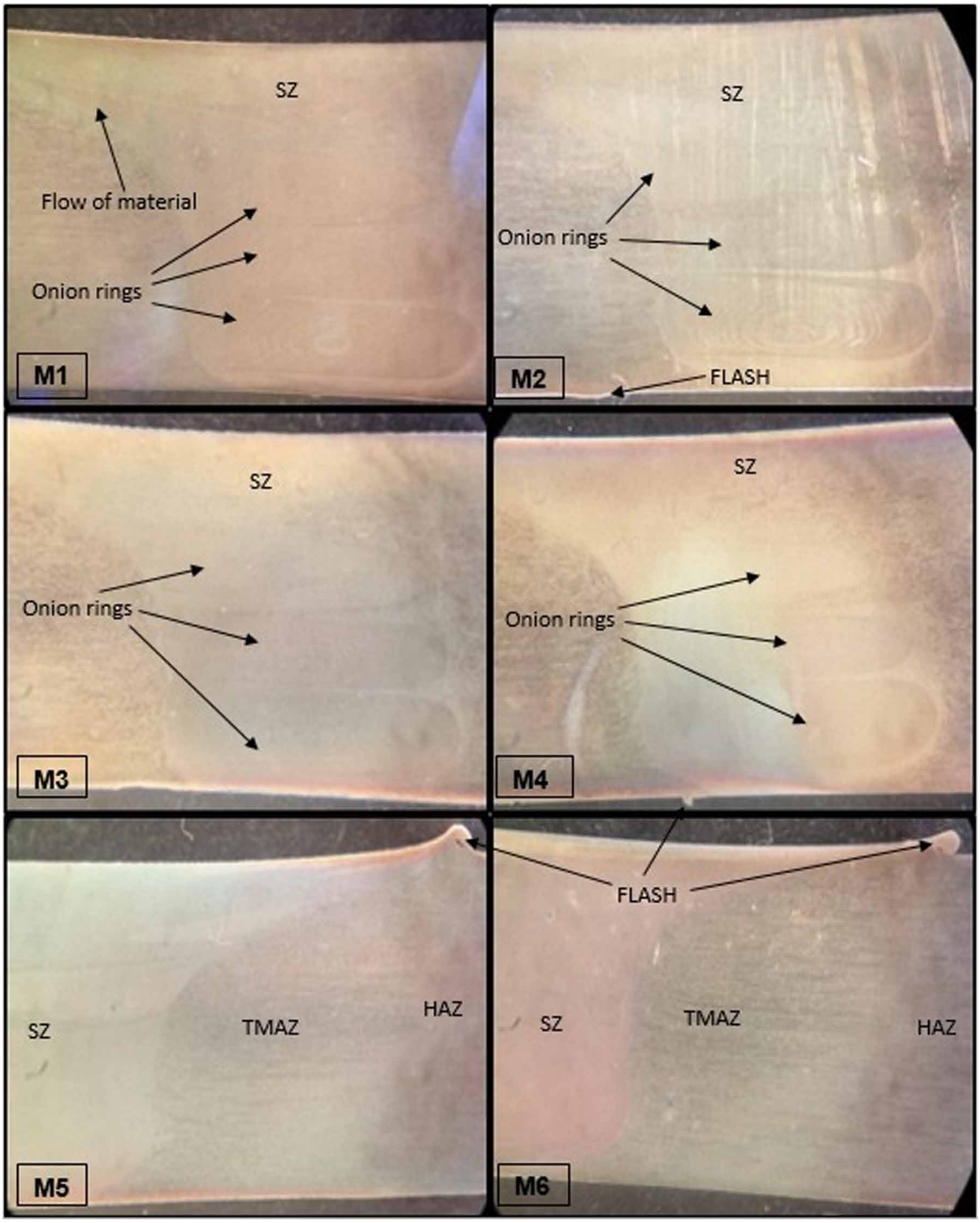

This behavior is caused by the distinct thermo-mechanical actions experienced by these three regions. The microstructural arrangement at the stir zone is influenced by the continuous recrystallization that is caused by the tool pin disruptive mechanical action during FSW. In other words, the refinement of grains is influenced by strain, strain rate, and temperature level (Su et al., 2003). On the other hand, the TMAZ region experiences heat flux that is coming from the rotating tool which leaves this zone

Figure 5. The macrostructural appearance of the specimens sampled at the end of the plate for all the speeds

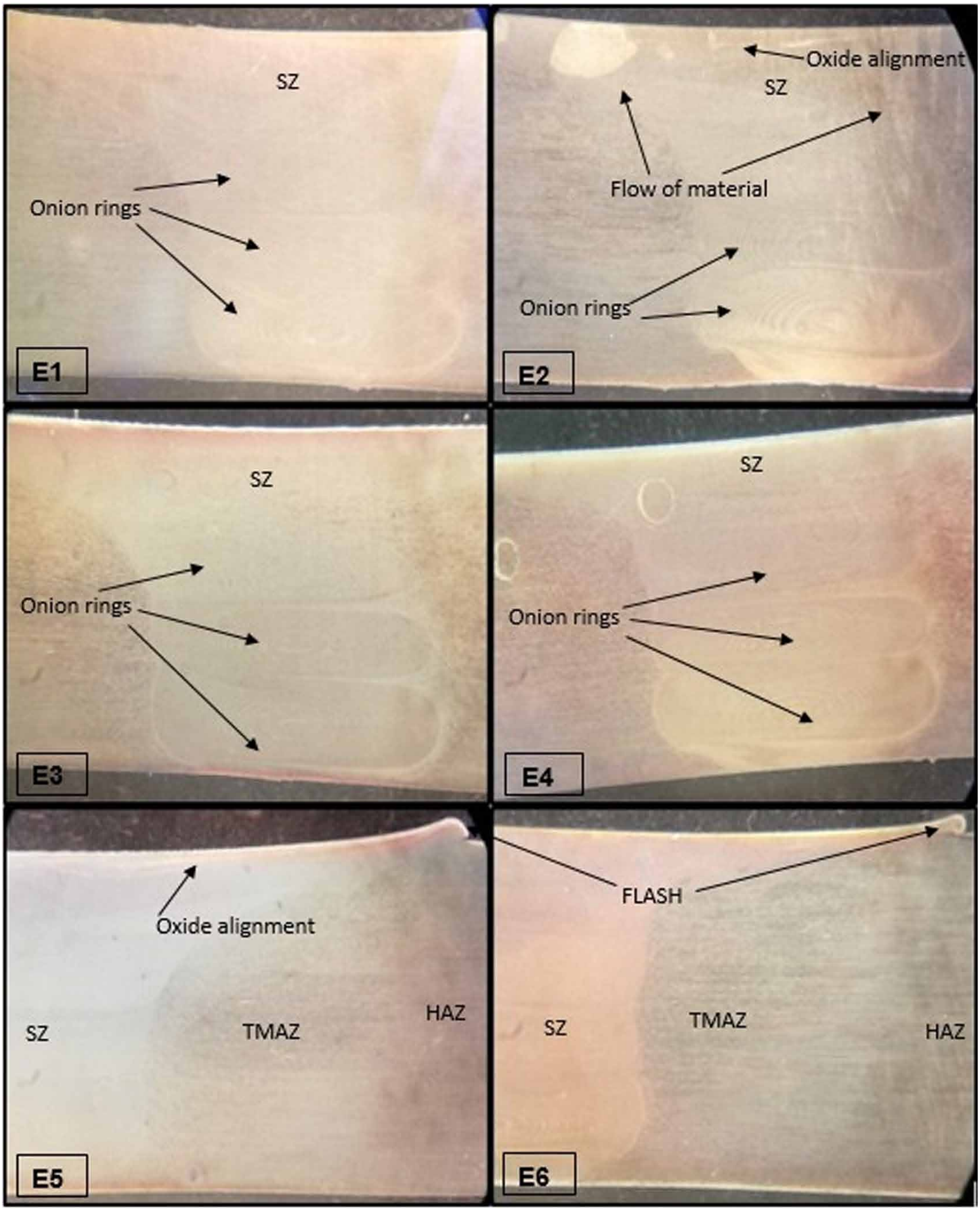

severely plastic deformed without recrystallization (elongated grains). The HAZ region experiences a thermal cycle that affects the microstructure and mechanical properties (Sabari et al., 2016; da Silva et al., 2011; Fratini & Buffa, 2005). Figure 6(a) – (c) shows the grain growth from the stir zone to the HAZ regions and this grain growth is due to the phenomenon explained earlier. This grain growth contributes towards the mechanical response of the material, however, the response differs

Figure 6a. The average grain size for the specimens sampled from the start on the weld of all the speeds

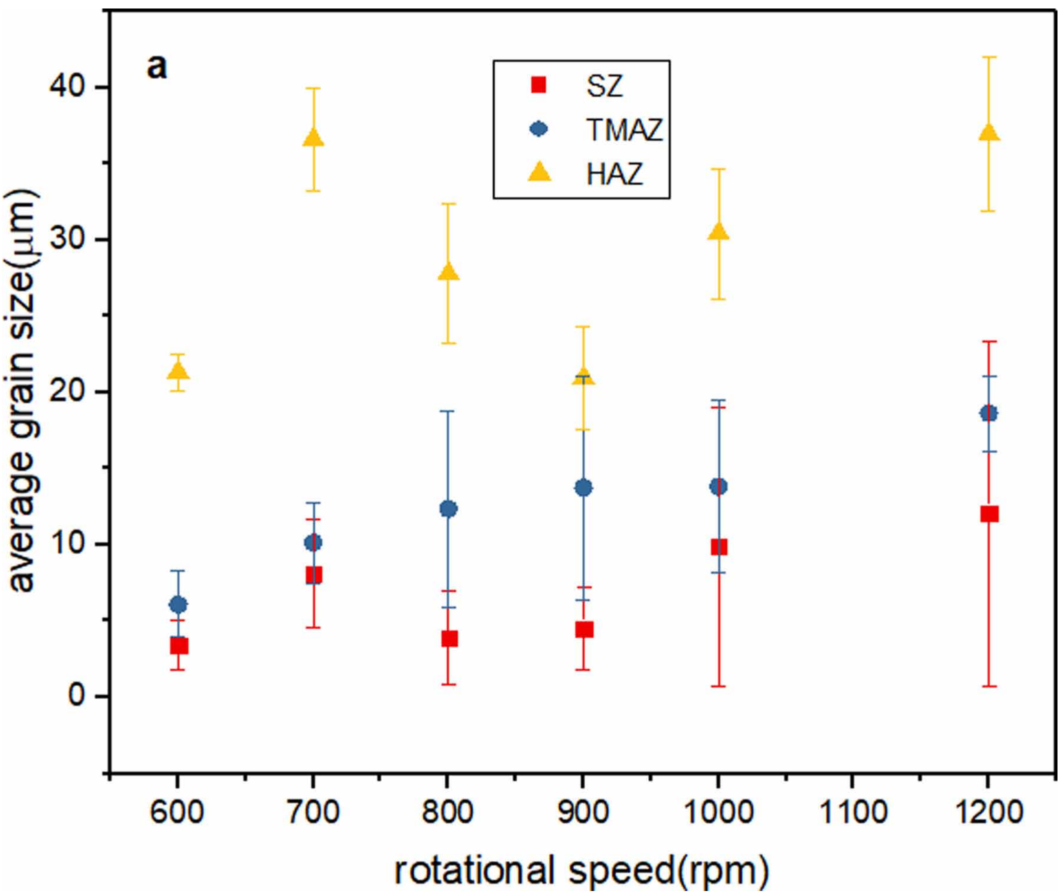

with materials (Singh et al.,2017; Orłowska et al.,2020; Yang et al., 2019). Lastly, the grain size at the three locations of the weld was found to be less than that of the parent material (51.63 μm).

Tensile Properties

Figure 7 shows the specimens of all the weld locations of all rotational speeds. The specimens sampled at the start of the weld for the rotational speed of 600 rpm(S1) failed at the SZ while the other two specimens (M1 and E1) failed outside the SZ i.e. HAZ region. The failure of S1 in this region is suggested to be caused by the defect that was identified in Figure 3 (S1). The failure of M1 and E1 at the HAZ region is caused by the coarse grains found in these regions (see Figure 6) (Yang et al., 2019; Sharma et al.,2019; Sameer & Birru, 2019). A similar trend is observed from specimens produced at a rotational speed of 700 rpm. However, it is not clear influenced the SZ failure o these specimens as there were no defects detected at the surface of these joints. All the other specimens failed at the HAZ region and this is due to the coarseness of grains found in this region.

Figure 8 shows the ultimate tensile strength (UTS) and percentage elongation as a function of rotational speed. The tensile behavior differs with the rotational speed. The ultimate tensile strength for M1 was found to be higher compared to S1 and E1. However, the percentage elongation for the same specimen was found to be lower than that of E1 and S1. This phenomenon can be attributed to the grain size phenomenon observed in Figure 6. S2 possesses higher UTS compared to M2 and E2, on the other hand, S2 possesses the lowest percentage elongation compared to E2 and M2. The UTS

Figure 6b. Average grain size of specimens sampled from the middle and the end of the weld

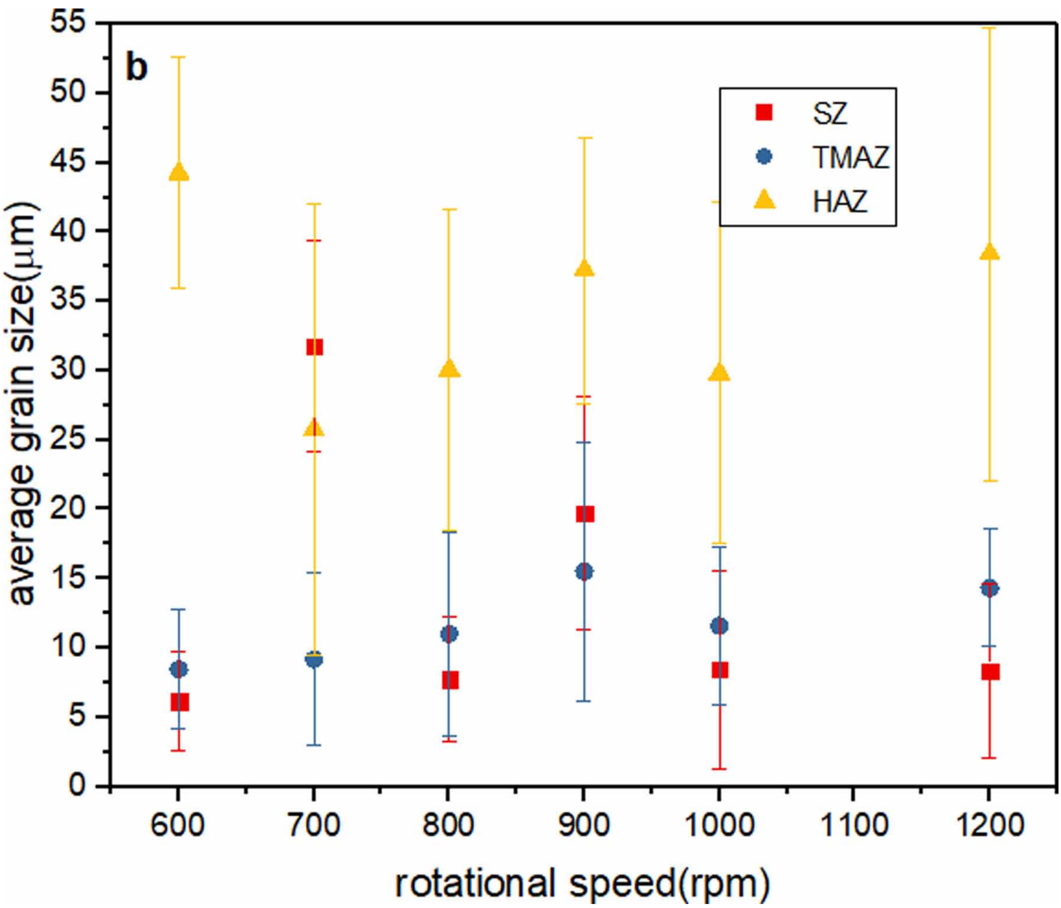

for S3 and S4 was found to be higher compared to that of M3, M4, E3, and E4 and this behavior is attributed to the grain size refinement associated with the said specimens (see Figure 6). The UTS of E5 and E6 was found to be higher than that of S5, M5, S6, and M6 and this is in agreement with the SZ grains of the said specimens. The specimens with high UTS tend to behave contrary in terms of percentage elongation (see Figure 8) and this behavior correlates with the one reported in the literature (Salih et al.,2020; Bocchi et al.,2018; Sharma et al.,2019). In as much as the specimens follow the trend reported in the literature, however, S4 has higher UTS and percentage elongation compared to M4 and E4 and this is contrary to the norm. This behavior is suggested to be influenced by the precipitate phenomenon (Tamadon et al., 2018, Sameer & Birru, 2019).

Fractography Analysis

The post tensile samples were all prepared for the fractographic analysis. It should be noted that all the fractured specimens shown in Figure 7 were all analyzed but only the specimens corresponding to the low speed (600 rpm) and the highest speed (1200 rpm) were included in this work. Two sets of fractured surfaces were included in this work since all the surfaces show similar surface morphology. Figure 9 (a) –(c) shows the surface morphology of the fractured specimens corresponding to the rotational speed of 600 rpm while Figure 9 (d) – (f) depicts the morphology of specimens corresponding to 1200 rpm. All the fractured surfaces revealed a cup-like dimpled surface that characterizes the

Figure 6c. Average grain size of specimens sampled from the middle and the end of the weld

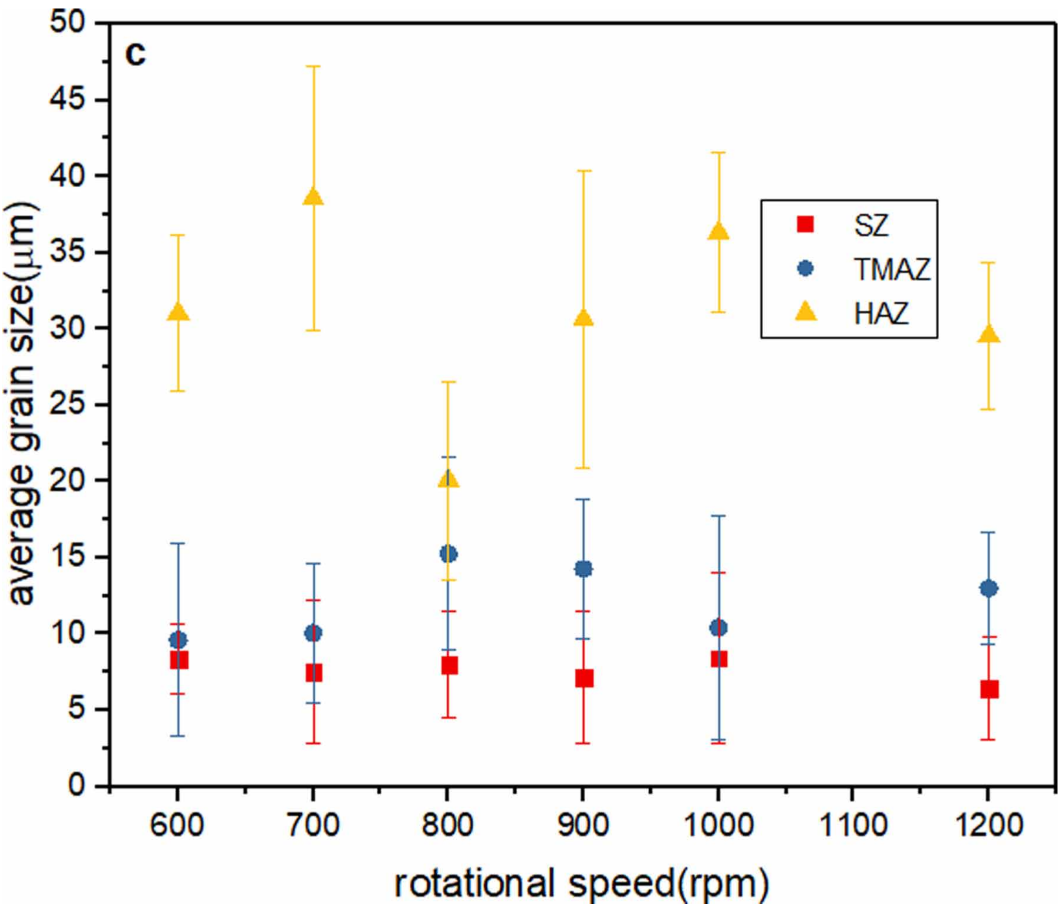

ductile failure mode (Msomi et al., 2020; Raturi et al., 2019; Thilagham & Muthukumaran, 2020; Chanakyan et al., 2020; Swaminathan et al., 2020). It should be noted that the dimple size was not measured hence it is not included in this work.

Microhardness Results

The microhardness results for all the speeds are presented in Figure 10. Figure 10(a) shows the microhardness results of the specimens extracted at the beginning of the weld for all the rotational speeds. The microhardness profile for specimens extracted in the middle and the end of the weld is shown in Figure 10 (b) and (c). All the specimens show a typical 'W' profile irrespective of the rotational speed and the sampling location from the weld. The microhardness is higher at the stir zone and declines towards the TMAZ with a sharp decline observed around the HAZ region. The decrease in microhardness is attributed to the grain size phenomenon defined by the Hall-Petch relation (Ahmed et al., 2017; Li et al.,2019). The other factor that may have contributed to the decline in microhardness is the thermal softening which is related to dissolution and coarsening of the strengthening precipitates (Li et al.,2019; Shen et al., 2014; Cao et al., 2016). The literature shows that the increase in microhardness is the grain size phenomenon. However, the specimens corresponding to the rotational speed of 700 rpm show a consistent decline at the center of the joint. This behavior is suggested to be influenced by the lack of thick intermetallic compound and the dissolution of precipitate which normally contributes towards the microhardness enhancement (Sameer and Birru, 2019).

Figure 7. The post tensile samples were all prepared for the fractographic analysis. It should be noted that all the fractured specimens

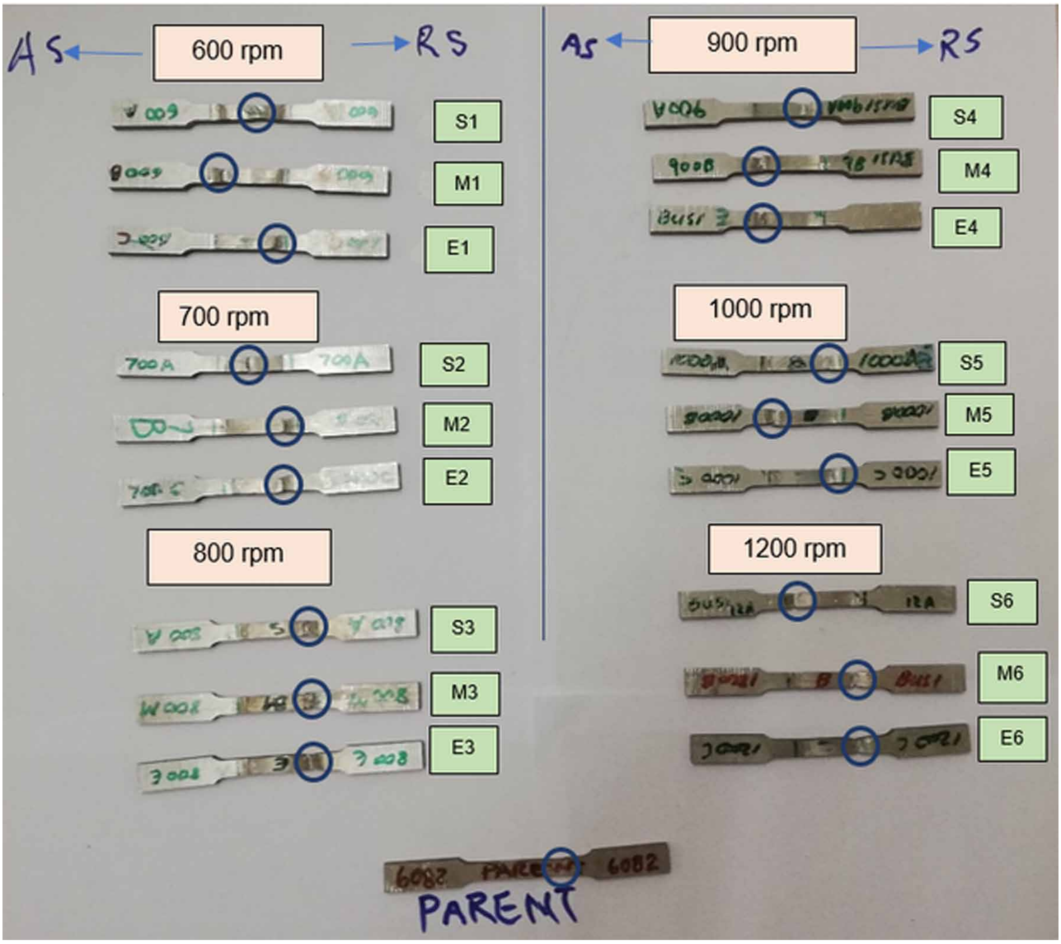

CONCLUSION

The influence of rotational speed on the friction stir welded similar joint was successfully investigated. The following conclusions can be drawn from this study:

- The variation in grain size influenced the tensile strength and the microhardness of the joint.
- The low rotational speed specimens showed good tensile properties compared to higher rotational speed.
- There was a notable coarsening of grains from the center of the SZ towards the HAZ region and this caused the specimens to fail consistently at the HAZ region.
- There was also a notable dependency on the mechanical properties of the sample with the specimen sampling location i.e. the specimens sampled at the center were mostly showing good tensile properties compared to specimens sampled from other locations of the weld.
- The rotational speed of 600 rpm combined with the traverse speed of 80 mm/min could be used to achieve good tensile properties of the AA6082-T6 similar joint.

Figure 8a. The specimens with high UTS tend to behave contrary in terms of percentage elongation

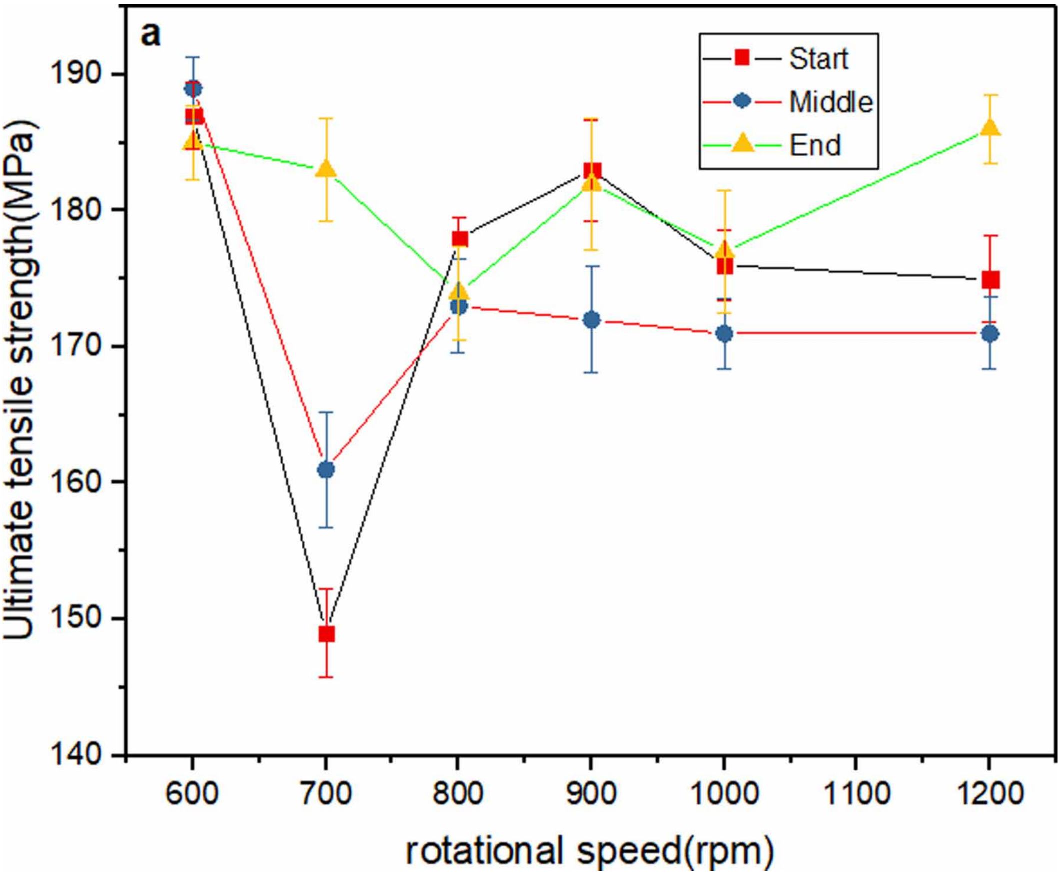

ACKNOWLEDGMENT

The authors would like to thank the National Research Foundation for financial support through Thuthuka Grant [118046]. DATA STATEMENT: The data used in producing this paper can be obtained from the corresponding author on request.

Figure 8b. The specimens with high UTS tend to behave contrary in terms of percentage elongation

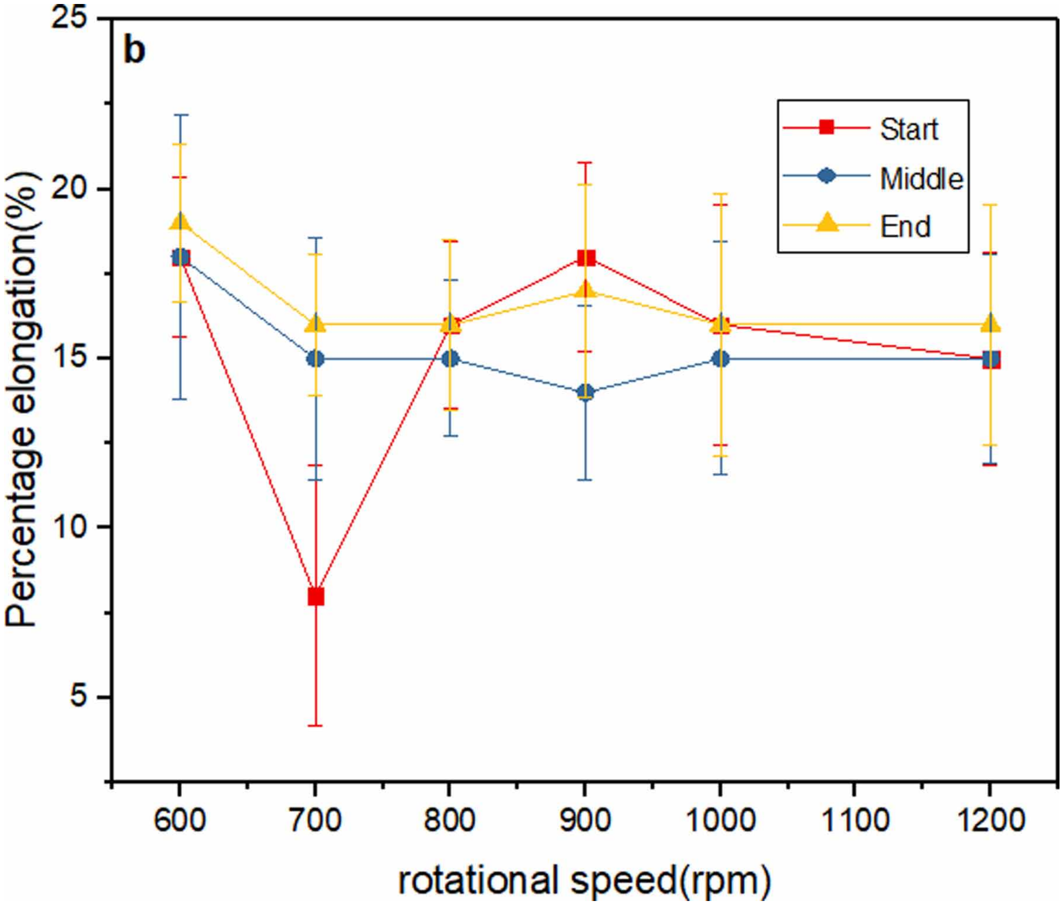

Figure 9. (a)–(c) shows the surface morphology of the fractured specimens corresponding to the rotational speed of 600 rpm (d) – (f) depicts the morphology of specimens corresponding to 1200 rpm

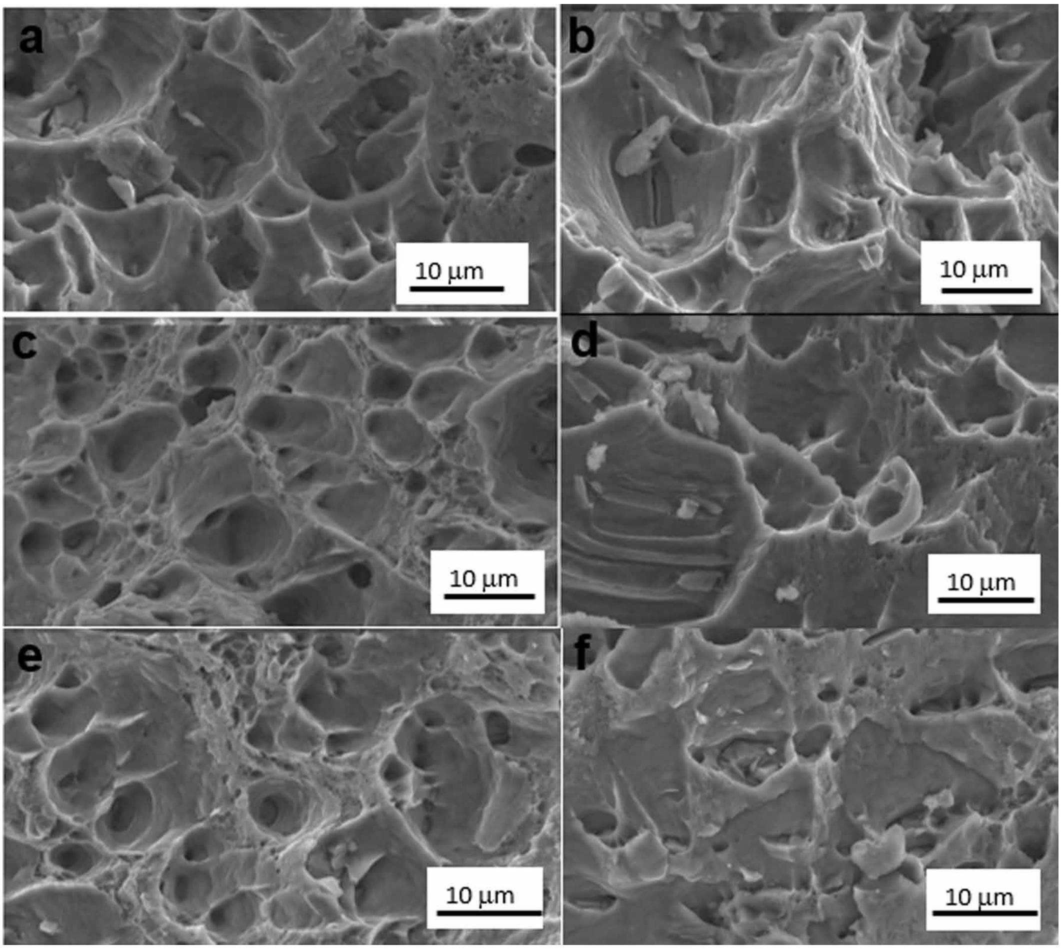

Figure 10a. Microhardness results of the specimens extracted at the beginning of the weld for all the rotational speeds

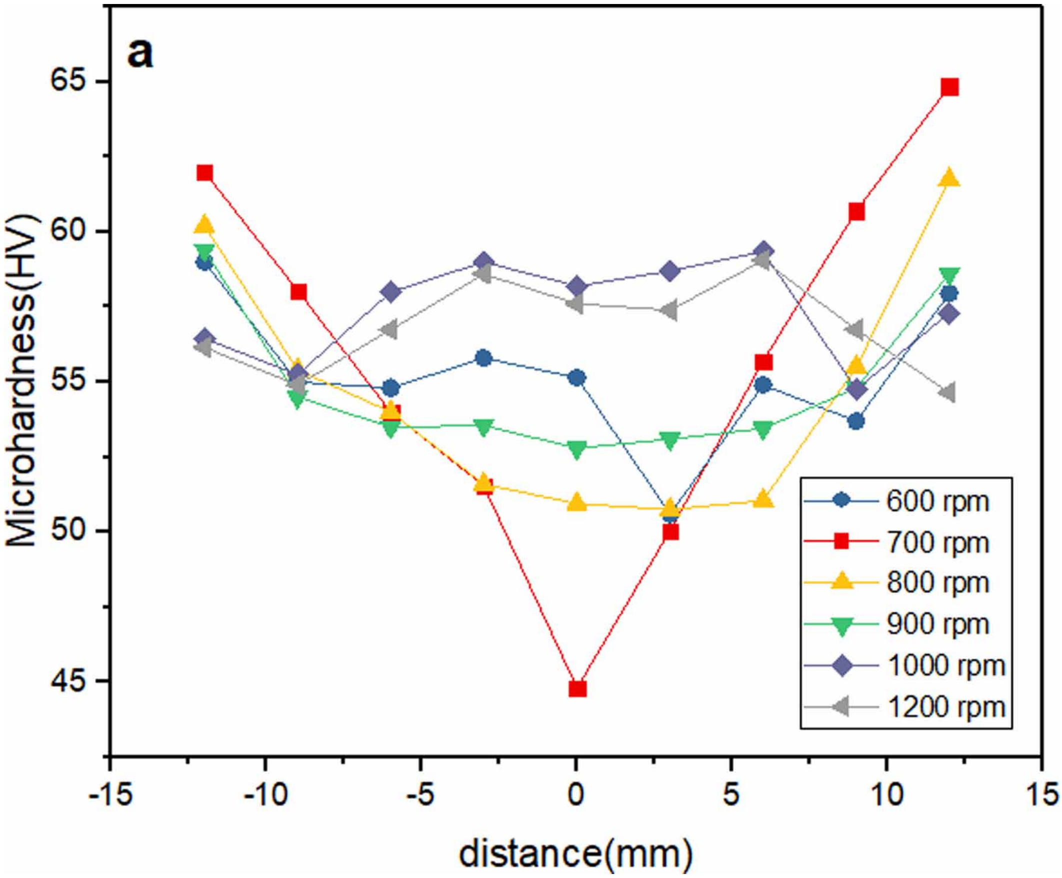

Figure 10b. The microhardness profile for specimens extracted in the middle and the end of the weld

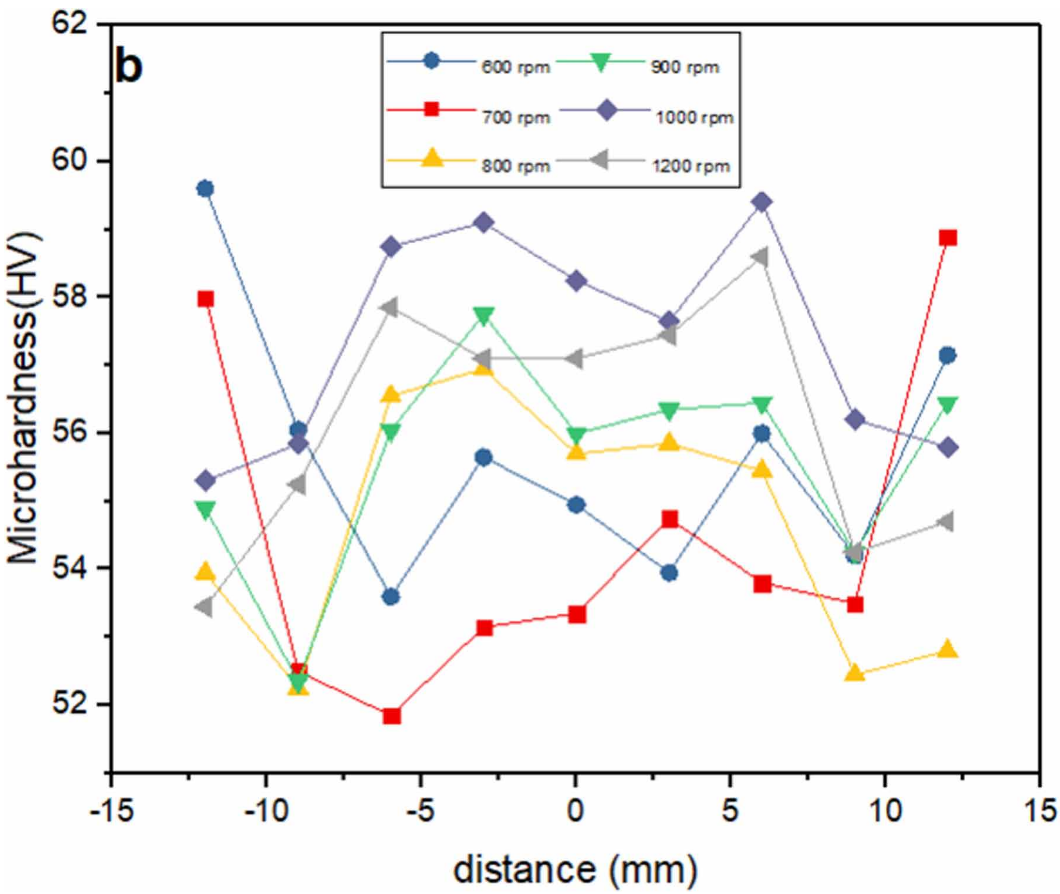

Figure 10c. The microhardness profile for specimens extracted in the middle and the end of the weld

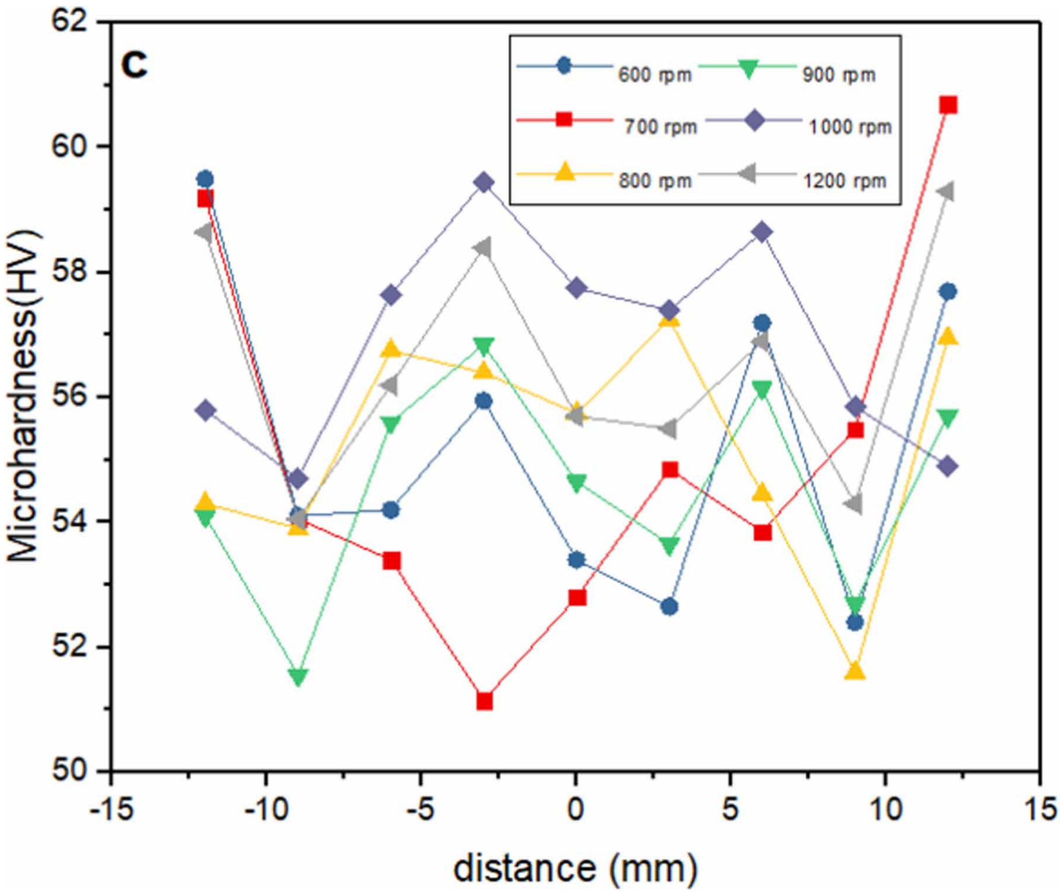

REFERENCES

Acharya, U., Roy, B. S., & Saha, S. C. (2020). Effect of tool rotational speed on the particle distribution in friction stir welding of AA6092/17.5 SiCp-T6 composite plates and its consequences on the mechanical property of the joint. *Defence Technology*, *16*(2), 381–391. doi:10.1016/j.dt.2019.08.017

Adamowski, J., Gambaro, C., Lertora, E., Ponte, M., & Szkodo, M. (2007). Analysis of FSW welds made of aluminium alloy AW6082-T6. *Archives of Materials Science and Engineering*, *28*(8), 453–460.

Ahmed, K. E., Nagesh, B. M., Raju, B. S., Drakshayani, N. D., & Abhijit Sudhindra Chethan Holla, A. S. C. (2020). Studies on the effect of welding parameters for friction stir welded AA6082 reinforced with Aluminium Oxide. *Materials Today: Proceedings*, *20*(2), 108–119. doi:10.1016/j.matpr.2019.10.059

Ahmed, M. M. Z., Ataya, S., Seleman, M. M. E., Ammar, H. R., & Ahmed, E. (2017). Friction stir welding of similar and dissimilar AA7075 and AA5083. *Journal of Materials Processing Technology*, *242*, 77–91. doi:10.1016/j.jmatprotec.2016.11.024

Boccarusso, L., Atarita, A., Carlone, P., Scherillo, F., Rubino, F., & Squillace, A. (2019). Dissimilar friction stir lap welding of AA 6082 - Mg AZ31: Force analysis and microstructure evolution. *Journal of Manufacturing Processes*, *44*, 376–388. doi:10.1016/j.jmapro.2019.06.022

Bocchi, S., Cabrini, M., D'Urso, G., Giardini, C., Lorenzi, S., & Pastore, T. (2018). The influence of process parameters on mechanical properties and corrosion behavior of friction stir welded aluminum joints. *Journal of Manufacturing Processes*, *35*, 1–15. doi:10.1016/j.jmapro.2018.07.012

Cao, J. Y., Wang, M., Kong, L., & Guo, L. J. (2016). Hook formation and mechanical properties of friction spot welding in alloy 6061-T6. *Journal of Materials Processing Technology*, *230*, 254–262. doi:10.1016/j.jmatprotec.2015.11.026

Chanakyan, C., Sivasankar, S., Meignanamoorthy, M., Ravichandran, M., & Muralidharan, T. (2020). Experimental investigation on influence of process parameter on friction stir processing of AA6082 using response surface methodology. *Materials Today: Proceedings*, *21*(1), 231–236. doi:10.1016/j.matpr.2019.05.384

Ciccarelli, D., El Mehtedi, M., Forcellese, A., Greco, L., & Simoncini, M. (2018). In-process control of rotational speed in friction stir welding of sheet blanks with variable mechanical properties. *Procedia CIRP*, *67*, 440–445. doi:10.1016/j.procir.2017.12.239

da Silva, A. A. M., Arruti, E., Janeiro, G., Aldanondo, E., Alvarez, P., & Echeverria, A. (2011). Material flow and mechanical behaviour of dissimilar AA2024-T3 and AA7075-T6 aluminium alloys friction stir welds. *Materials & Design*, *32*(4), 2021–2027. doi:10.1016/j.matdes.2010.11.059

Das, U., & Toppo, V. (2018). Effect of Tool Rotational Speed on Temperature and Impact Strength of Friction Stir Welded Joint of Two Dissimilar Aluminum Alloys. *Engineering Failure Analysis*, *96*, 570–588.

Fratini, L., & Buffa, G. (2005). CDRX modeling in friction stir welding of aluminium alloys. *International Journal of Machine Tools & Manufacture*, *45*(10), 1188–1194. doi:10.1016/j.ijmachtools.2004.12.001

Guo, Y., Ma, Y., & Wang, F. (2019). Dynamic fracture properties of 2024-T3 and 7075-T6 aluminum friction stir welded joints with different welding parameters. *Theoretical and Applied Fracture Mechanics*, *104*, 102372. doi:10.1016/j.tafmec.2019.102372

Kumar, H. M. A., & Ramana, V. V. (in press). Influence of tool parameters on the tensile properties of friction stir welded aluminium 5083 and 6082 alloys. *Materials Today: Proceedings*.

Kumar, S., Srivastava, A. K., Singh, R. K., & Dwivedi, S. P. (2020). Experimental study on hardness and fatigue behavior in joining of AA5083 and AA6063 by friction stir welding. *Materials Today: Proceedings*, *25*(4), 646–648.

Maneiah, D., Mishra, D., Rao, K. P., & Raju, K. B. (2020). Process parameters optimization of friction stir welding for optimum tensile strength in Al 6061-T6 alloy butt welded joints. *Materials Today: Proceedings*, *5*(2), 6170–6175. doi:10.1016/j.matpr.2020.01.215

Mishra, R. S., & Ma, Z. Y. (2005). Friction stir welding and processing. *Materials Science and Engineering R Reports*, *50*(1–2), 1–78. doi:10.1016/j.mser.2005.07.001

Moshwan, R., Yusof, F., Hassan, M. A., & Rahmat, S. M. (2015). Effect of tool rotational speed on force generation, microstructure and mechanical properties of friction stir welded Al – Mg – Cr – Mn (AA5052-O) alloy. *Materials & Design*, *66*, 118–128. doi:10.1016/j.matdes.2014.10.043

Msomi, V., & Mbana, N. (2020). Mechanical Properties of Friction Stir Welded AA1050-H14 and AA5083-H111 Joint: Sampling Aspect. *Metals*, *10*(214), 1–17. doi:10.3390/met10020214

Msomi, V., Mbana, N., & Mabuwa, S. (2020). Microstructural analysis of the friction stir welded 1050-H14 and 5083-H111 aluminium alloys. *Materials Today: Proceedings*, *26*(2), 189–192. doi:10.1016/j.matpr.2019.10.038

Nagu, K., & Kumar, A. (in press). Effect of tool rotational speed on microstructure and mechanical properties of friction stir welded AA6061-T6 alloy using brass interlayer. *Materials Today: Proceedings*.

Orłowska, M., Olejnik, L., Campanella, D., Buffa, G., Morawiński, L., Fratini, L., & Lewandowska, M. (2020). Application of linear friction welding for joining ultrafine grained aluminium. *Journal of Manufacturing Processes, 56*(A), 540-549.

Palani, K., Elanchezhian, C., Ramnath, B. V., Bhaskar, G. B., & Naveen, E. (2018). Effect of pin profile and rotational speed on microstructure and tensile strength of dissimilar AA8011, AA01-T6 friction stir welded aluminum alloys. *Materials Today: Proceedings*, *5*(11), 24515–24524. doi:10.1016/j.matpr.2018.10.248

Ramnath, B. V., Elanchezhian, C., Rajesh, S., Prakash, S. J., Kumaar, B. M., & Rajeshkannan, K. (2018). Design and Development of Milling Fixture for Friction Stir Welding. *Materials Today: Proceedings*, *5*(1), 1832–1838. doi:10.1016/j.matpr.2017.11.282

Ratnam, C. H., Kumar, B. S., & Rohinikumar, C. H. (2019). Investigation of the Influence of Twin Pin Tool Geometry in Friction Stir Welding of Dissimilar Al alloys. *Materials Today: Proceedings*, *18*(7), 5100–5106. doi:10.1016/j.matpr.2019.07.506

Raturi, M., Garg, A., & Bhattacharya, A. (2019). Joint strength and failure studies of dissimilar AA6061-AA7075 friction stir welds: Effects of tool pin, process parameters and preheating. *Engineering Failure Analysis*, *96*, 570–588. doi:10.1016/j.engfailanal.2018.12.003

Raturi, M., Garg, A., & Bhattacharya, A. (in press). *Joint strength and failure studies of dissimilar AA6061-AA7075 friction stir welds: Effects of tool pin, process parameters and preheating*. Academic Press.

Sabari, S. S., Malarvizhi, S., & Balasubramanian, V. (2016). Influences of tool traverse speed on tensile properties of air-cooled and water-cooled friction stir welded AA2519-T87 aluminium alloy joints. *Journal of Materials Processing Technology*, *237*, 286–300. doi:10.1016/j.jmatprotec.2016.06.015

Safeen, M. W., & Spena, P. R. (2019). Main issues in quality of friction stir welding joints of aluminum alloy and steel sheets. *Metals*, *9*(5), 610. doi:10.3390/met9050610

Salih, O. S., Neate, N., Ou, H., & Sun, W. (2020). Influence of process parameters on the microstructural evolution and mechanical characterisations of friction stir welded Al-Mg-Si alloy. *Journal of Materials Processing Technology*, *275*, 116366. doi:10.1016/j.jmatprotec.2019.116366

Sameer, M. D., & Birru, A. K. (2019). Mechanical and metallurgical properties of friction stir welded dissimilar joints of AZ91 magnesium alloy and AA 6082-T6 aluminium alloy. *Journal of Magnesium and Alloys*, *7*(2), 264–271. doi:10.1016/j.jma.2018.09.004

Sharma, G., & Dwivedi, D. K. (2017). Study on microstructure and mechanical properties of dissimilar steel joint developed using friction stir welding. *International Journal of Advanced Manufacturing Technology*, *88*(5–8), 1299–1307. doi:10.1007/s00170-016-8763-5

Sharma, S., Handa, A., Singh, S. S., & Verma, D. (2019). Influence of tool rotation speeds on mechanical and morphological properties of friction stir processed nano hybrid composite of MWCNT-Graphene-AZ31 magnesium. *Journal of Magnesium and Alloys*, *7*(3), 487–500. doi:10.1016/j.jma.2019.07.001

Shen, Z., Yang, X., Yang, S., Zhang, Z., & Yin, Y. (2014). Microstructure and mechanical properties of friction spot welded 6061-T4 aluminum alloy. *Materials & Design*, *54*, 766–778. doi:10.1016/j.matdes.2013.08.021

Silva-Magalhães, A., De Backer, J., Martin, J., & Bolmsjö, G. (2019). In-situ temperature measurement in friction stir welding of thick section aluminium alloys. *Journal of Manufacturing Processes*, *39*, 12–17. doi:10.1016/j.jmapro.2019.02.001

Singh, G., Kang, A. S., Singh, K., & Singh, J. (2017). Experimental comparison of friction stir welding process and TIG welding process for 6082-T6 Aluminium alloy. *Materials Today: Proceedings*, *4*(2), 3590–3600. doi:10.1016/j.matpr.2017.02.251

Soni, N., & Chandrashekhar, S., A., K., & V.R., C. (2017). Defects Formation during Friction Stir Welding: A Review. *International Journal of Engineering and Management Research*, *7*(3), 121–125.

Su, J. Q., Nelson, T. W., Mishra, R., & Mahoney, M. (2003). Microstructural investigation of friction stir welded 7050-T651 aluminium. *Acta Materialia*, *51*(3), 713–729. doi:10.1016/S1359-6454(02)00449-4

Sunilkumar, D., Muthukumaran, S., Vasudevan, M., & Madhusudan Reddy, G. (2020). Tool rotational speed variant response on the evolution of microstructure and its significance on mechanical properties of friction stir welded 9Cr-1Mo steel. *Journal of Materials Processing Technology*, *278*, 116536. doi:10.1016/j.jmatprotec.2019.116536

Swaminathan, G., & Sathiyamurthy, S. (2020). Domination of process control parameters on tensile properties of friction stir welding of AA7075/AA6101 alloys. *Materials Today: Proceedings*, *22*(3), 639–648. doi:10.1016/j.matpr.2019.09.034

Taheri, H., Kilpatrick, M., Norvalls, M., Harper, W. J., Koester, L. W., Bigelow, T., & Bond, L. J. (2019). Investigation of nondestructive testing methods for friction stir welding. *Metals*, *9*(6), 1–22. doi:10.3390/met9060624

Tamadon, A., Pons, D. J., Sued, K., & Clucas, D. (2018). Thermomechanical grain refinement in AA6082-T6 thin plates under bobbin friction stir welding. *Metals*, *8*(375), 1–20. doi:10.3390/met8060375

Thilagham, K. T., & Muthukumaran, S. (2020). Process parameter optimization and characterization studies of dissimilar friction stir welded advancing side AA6082-T6 with retreating side AA2014-T87. *Materials Today: Proceedings*, *27*, 2513–2519. doi:10.1016/j.matpr.2019.09.228

Thilagham, K. T., & Muthukumaran, S. (2020). Process parameter optimization and characterization of friction stir welded advancing side AA6082-T6 with retreating side AA7075-T651. *Materials Today: Proceedings*, *27*, 2260–2264. doi:10.1016/j.matpr.2019.09.108

Tongne, A., Desrayaud, C., Jahazi, M., & Feulvarch, E. (2016). *On material flow in Friction Stir Welded Al alloys.* Academic Press.

Unnikrishnan, M. A., & Dhas, E. R. J. (2017). A Survey on Friction Stir Welding of Dissimilar Magnesium Alloys. *IOP Conference Series. Materials Science and Engineering*, *247*(1), 012009. doi:10.1088/1757-899X/247/1/012009

Yang, M., Bao, R., Liu, X., & Song, C. (2019). Thermo-mechanical interaction between aluminum alloy and tools with different profiles during friction stir welding. *Transactions of Nonferrous Metals Society of China*, *29*(3), 495–506. doi:10.1016/S1003-6326(19)64958-7

Yang, X., Feng, W., Li, W., Dong, X., Xu, Y., Chu, Q., & Yao, S. (2019). Microstructure and properties of probe less friction stir spot welding of AZ31 magnesium alloy joints. *Transactions of Nonferrous Metals Society of China*, *29*(11), 2300–2309. doi:10.1016/S1003-6326(19)65136-8

Zhang, C., Huang, G., Cao, Y., Zhu, Y., & Liu, Q. (2019). On the microstructure and mechanical properties of similar and dissimilar AA7075 and AA2024 friction stir welding joints: Effect of rotational speed. *Journal of Manufacturing Processes*, *37*, 470–487. doi:10.1016/j.jmapro.2018.12.014

Velaphi Msomi received his DTech in Mechanical Engineering at Cape Peninsula University of Technology in 2015. He started supervising undergraduate and Postgraduate students in various projects. He became the Head of Program for Diploma program. He is a leader of the research group called friction stir welding/processing group. He has authored and co-authored number of publications and book chapters in various topics.

Busiswa Tracey Jantjies is a lecturer at the Cape Peninsula University of Technology.